Presented at the AIAA Guidance, Navigation and Controls Conference, Keystone Colorado, August 21-24, 2006
Paper AIAA 2006-6336

Deployment Modeling of an Inflatable Solar Sail Spacecraft

Nathan W. Graybeal[1] and James I. Craig[2]
Georgia Institute of Technology, Atlanta, GA, 30332

and

Mark S. Whorton[3]
Guidance, Navigation and Mission Analysis, NASA Marshall Space Flight Center

A simple model for the dynamic response of an inflatable solar sailcraft during deployment has been developed and tested for several distinct scenarios. The basic kinematics for the model were formulated in a deliberate manner that in future studies will allow systematic increases in model fidelity (and complexity) while at the same time leading to a straightforward implementation as a state space model in Matlab/Simulink. Despite the low order of the current model, clear trends were evident. The results expose the existence of deployment conditions that have a destabilizing effect on a flexible sailcraft which is not seen in a similar rigid-body spacecraft. Future work with higher order models will provide further insight into these conditions so that, ultimately, a robust deployment can be guaranteed.

I. Introduction

While the modern notion of solar sailing has been in the consciousness of the scientific community since the early part of the twentieth century, it was not until the 1970's that any substantial engineering efforts were applied to the problem. At that time, the uncertainties surrounding the high risk deployment of square solar sails removed them from popularity when compared to the simpler heliogyro. With more than three decades of gradual development, no solar sail has yet been flown but new materials technologies have stimulated renewed interest in the larger sails and tighter turning performance made possible by a square configuration.[1] Recent competition for funding in the area of solar sail spacecraft technology has led to the development of a new breed of advanced concepts coming closer in line to practical application than past efforts have achieved.

With current mission specifications mandating 10,000-m^2 of reflective area on a square sail for a nominal 1 AU mission, the scope of the new designs also far surpasses the size limitations of earlier efforts due to rapid advances in manufacture and strength of composite materials. A particular design of interest is under development by L'garde Inc, and stems from their company origin as a developer of inflatable modules for space missions. An inflatable structure presents unique challenges in the development of a functional solar sail spacecraft, due not only to the scaling of manufacturing efforts, but also the potential difficulties associated with the deployment of such a large vehicle. Additionally, the presence of large-scale inflatable components combined with the even larger gossamer sail introduces a daunting level of uncertainty in potential deployment models.

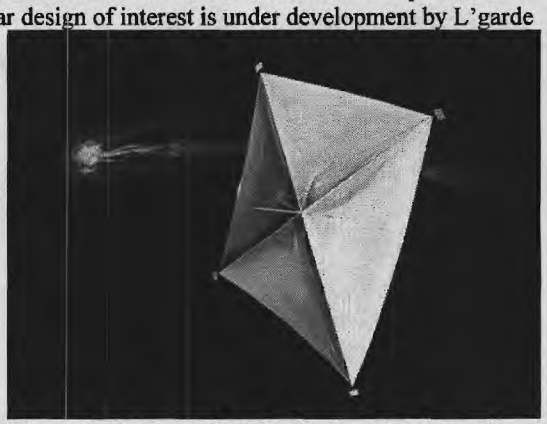

Figure 1. Concept sketch of a square solar sail.

Over the last several years numerous researchers have considered the complexities of inflatable structures from various standpoints. Clem, Smith, and Main[2,3] studied z-folded accordion-style deployment mechanisms of purely

[1] Graduate Research Assistant, Aerospace Engineering, Member AIAA.
[2] Professor, Aerospace Engineering, Senior Member AIAA.
[3] Branch Chief, AIAA Associate Fellow.

inflated (i.e., *not* rigidized) tubular beams. This work provided perspective on the nonlinear stiffness properties of inflatables under different inflation pressures, and is an excellent reference into the complexity of the problem, while focusing mostly on laboratory validation of a model for an inflated Kapton bladder.

Research by Smalley and Tinker[4] has also focused on the nonlinear phenomenon of inflated boom structural dynamics. While their work was limited to fully deployed structures, it did provide a powerful case for the accuracy of detailed finite-element analysis tools in attacking the problem of uncertainty in the analytical models for inflated structures. Additionally, this work was able to consider the effects of axial forces inside the strut due to inflation pressure. More recent work by JPL[5] has provided a characterization of the deployment of an aluminum laminate tube that is rolled around a tip mandrel for packing. During deployment the tube is inflated with gas causing it to unroll. Once extended, the tube is exposed to an increased internal pressure, removing any wrinkles from the aluminum and causing it to become a uniform rigid cylinder. This effort provided further insight into the severity of expected tip-mandrel vibration during an inflated deployment, but unfortunately it focused on a much less common concept of inflated aluminum tubing. In all, there is considerable evidence of the progress in the field, but at the same time, the presence of numerous concepts and a vast multitude of possible configurations does not lend well to the development of a "catch-all" solution for deployment.

As a practical example, the concept examined in this paper utilizes inflatable booms that are extruded, rather than unfolded, and contain a composite isogrid substructure that is impregnated with a sub-T_g resin that is rigidized after deployment. This system encapsulates the complexity of all of the previously discussed systems, with the additional difficulties of uncertain resistance during deployment due to friction in the folds (the folding method was chosen for its extremely high packing factor, *not* for its simplicity) and the fact that the booms must be heated during launch and deployment to allow them to remain soft until fully extruded. Possible failures run the gamut from physical asymmetry due to uncertain deployment methods, tears in the sail caused by entanglement due to packing tolerances, and loss of heating or pressure systems required for deployment. Careful ground testing in a vacuum with 10-m and 20-m systems has provided strong evidence that the concept is feasible, but they have also pointed out the likelihood of deployment anomalies. And despite evidence of regarding the predictability of the spacecraft's structural dynamics *after* deployment[6,7], a gap exists in the published work regarding the predictability of the structure *during* deployment.

While the difficulties of modeling the complete system developed by L'garde would be prohibitive due both to the complexity of the system and the proprietary nature of its specifications, it is certainly feasible to simplify the system in order to obtain an approximation of how severe certain failures can be. Thrust asymmetry is the most likely off-nominal condition to occur during even the best circumstances. This condition can stem from many causes, such as the four booms in a square sail not deploying at the same rate, tears forming in the sail, or unpacking difficulties, but the result is the same, i.e. the sail center of pressure becomes offset from the spacecraft center of mass. Fortunately, the possibility for overcoming this type of failure is strong if proper deployment procedures are in place to ensure a robust deployment event. The solutions can range from altering the method of deployment regulation to spin stabilization and each has unique benefits and pitfalls.

The purpose of this paper is to present a simplified model for the deployment dynamics of a square solar sail spacecraft, with an intent that is two-fold. Measures will be taken to show the effects of flexibility on the deployment sequence by comparing a rigid spacecraft model with a first-order flexible model. Additionally, different asymmetric configurations will be analyzed to determine the conditions surrounding a stable deployment. This simplified approach does not claim to provide all of the answers to the full-scale problem, but will provide insight into the trends associated with deployment failure, and it will identify conditions of interest for further evaluation with higher-order analysis.

II. Model Development

The goal of this work is to develop a model that simulates the inflation deployment of an extruding square solar sail spacecraft. It was clear from the beginning that large simplifications were required to start the groundwork for such a project, and a deliberate approach was taken to gradually employ higher levels of model fidelity. The primary focus of this paper is to describe the development of a low-order flexible dynamic model for the deploying spacecraft and compare the results with an earlier rigid-body deployment model. This comparison will demonstrate the trends behind a successful and robust deployment, while noting phenomenon unique to the flexible model.

A. Simplifications from the Actual System

The model simplifications fall into four major categories: simplifications to (1) the dynamic equations, (2) the physical geometry and inertia, (3) the thrust model, and (4) the flexibility model.

1. Dynamic Equations

The foremost assumption in the present model is placing the spacecraft in inertial space. At this point in the development process, it has allowed us to neglect definition of a clear orbit, the effects of gravity gradient and other effects imposed by orbital dynamics. The modularity of the model makes the supplemental introduction of any of these effects a relatively simple addition, but it was deemed appropriate to maintain as much clarity as possible in early work as to why certain outcomes are reached. Yaw-pitch-roll (3-2-1) Euler angles were used to represent the orientation of the spacecraft in the inertial frame of reference. The chosen orientation is depicted in Figure 2 with yaw (ψ_1) occurring first around the i_3-axis, pitch (ψ_2) occurring second around an intermediate i_2'-axis, and roll (ψ_3) occurring third around the i_1''-axis (coincident with the orientation of the b_1-axis of the body). While this transformation reaches a singularity at 90° of pitch, it is a trivial case because spacecraft failure due to extreme attitude is considered to occur at 45° of either pitch or roll. This failure condition is derived from physical limitations to produce correcting torques due to the rapid decline in solar pressure at such high angles of attack.

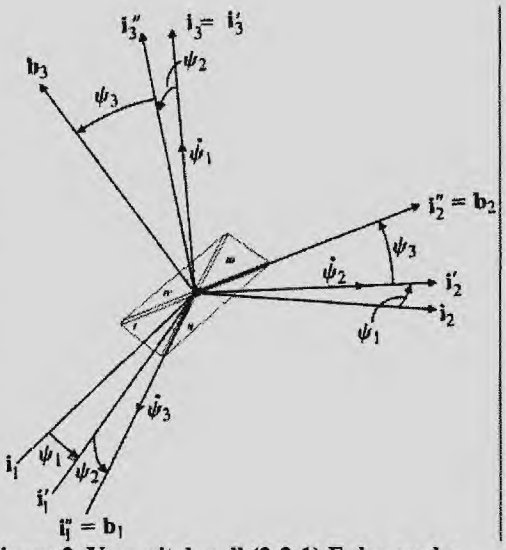

Figure 2. Yaw-pitch-roll (3-2-1) Euler angles.

2. Physical Geometry and Inertia

Given the scope of the system proposed by L'garde, some generalizations were necessary to capture the approximate geometry of the spacecraft. Care was taken to incorporate as many of the actual physical properties as possible during the process, though the geometry was simplified to the greatest extent possible for the purposes of expedient mass-moment-of-inertia calculations. The central bus was considered to have inertial properties reasonable for the mass given by the system specifications at a radius of gyration considered reasonable for the geometry of the actual system.

The deployed region of each of the four booms, running the semi-diagonal of the square sail, is approximated as a uniform cylindrical tube with the mass computed by utilizing the published linear density for the proposed spacecraft. This approximation should represent with reasonable accuracy the mass distribution of the internal Kapton bladder and external Mylar skin, although it clearly neglects certain aspects of the internal isogrid, a component with a proprietary layout that would be difficult to account for completely, in any case. Additionally, the external truss system commonly depicted on concept sketches[1] of this type of square solar sail is neglected for simplicity at this stage of the process, as it is hoped by some that a system that contributes so heavily to deployment failure would ultimately not be required by the final mission design.

The deployed portion of each sail quadrant is approximated as a 2-μm thick triangular plate for the purposes of determining mass distribution. The published areal density of the sail material (a film of Mylar, coated on one side with aluminum and coated with black chrome on the other) was utilized for maximum coherence to the final configuration. Possible in-plane deformation of the sail quadrant is neglected for simplicity, with this assertion supported by the relatively low mass of the sail when compared to the rest of the spacecraft and the very high tension in the sail plane.

The internal deployment mandrel, undeployed boom material, and some portion of the undeployed sail membrane adjacent to each boom is assumed to be consolidated at the tip of each boom. The conglomerate is approximated to be contained in a solid cylindrical volume, similar in radius to the tubular approximation for the deployed structure. The mandrel mass was approximated with a similar linear density to the booms due to its makeup as a simple inflatable bladder, while published values were, once again, used for the sail and boom materials. Tip vanes, another common feature of the aforementioned concepts[1], were also neglected, again, due to their hopeful removal from a final design. It would be relatively simple to account for such a feature in the current model by simply increasing the mandrel mass appropriately to attribute the inertia associated with such a system properly.

Finally, the undeployed sail material folded at the edge of the sail quadrant was approximated as a thin rectangular plate with a thickness similar to the deployed sail, a width of the tip mandrel, and a length of the

deployed sail edge. Such an approximation of shape makes a negligible difference in the computed mass-moment-of-inertia when compared to the actual trapezoidal shape of the stowed section.

In total, while the model developed for the spacecraft mass distribution is just an approximation, it should remain accurate to within a reasonable tolerance, due to the clean geometric shapes prevalent in the spacecraft configuration. Additionally, for the overall fidelity of the final model to be weighted so heavily towards the calculation of mass-moments-of-inertia would artificially bottleneck the process when compared with the altogether cruder approximations associated with the low-order flexibility currently taken into account.

3. Thrust Model

For the purpose of thrust calculation, the sail quadrants are considered to be perfectly flat and completely reflective. This removes the need to consider the loss of thrust due to wrinkles which can lead to reduction in actual sail performance. The flat quadrants are of identical geometry to that used for the calculation of mass properties, and solar pressure is assumed to be uniform across their surface, with a center of pressure collocated with the quadrant center of mass. The solar pressure (approximately 9-$\mu N/m^2$) is based on largely accepted values for thrust producible by an optimal sail design[1] at a distance from the Sun of 1 AU. Only the component of thrust normal to a sail quadrant is considered (reference Fig. 3). This assumption neglects the tangential forces due to electromagnetic effects[1]. Finally, the tip vanes are once again neglected for the purpose of thrust calculation to be consistent with the mass calculation and because they would only contribute thrust after a complete deployment, were they incorporated.

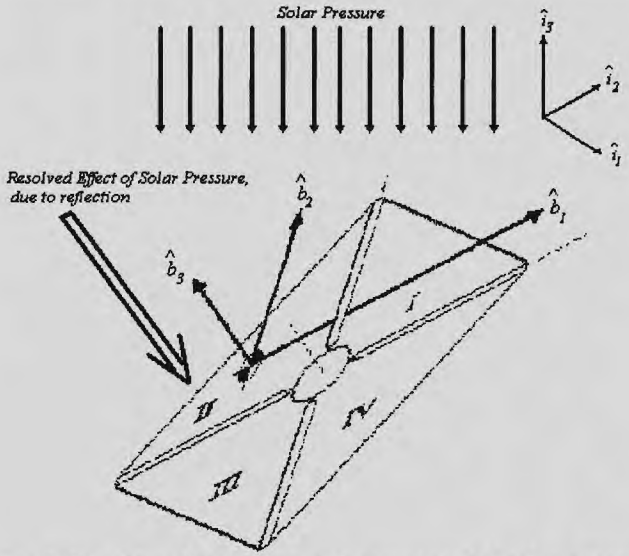

Figure 3. Direction of body-oriented component of solar pressure.

4. Flexibility Model

A first-order approximation of flexibility has been introduced into the model by allowing the booms to rotate with a single degree-of-freedom at their respective roots and by providing a reaction moment with a rotational spring. The resulting motion can be envisioned as a set of flapping rotor blades with lead-lag motion not allowed. The omission of lead-lag motion in the current flexibility model is supported by preliminary finite element analyses that show the majority of motion (greater than 95%) to be in the direction of flapping deformation. This suppression of lead-lag deflection is thought to come from the presence of restraining tensile forces in the sail supports that effectively maintain the position of the booms in that plane of motion. By using the equations of motion with a similar derivation to a spinning rotor, it will be a relatively straightforward exercise to later add lead-lag motion once a higher fidelity flexible model is implemented.

B. Equations of Motion

A modular approach was taken for the development of the equations of motion describing the deployment of a square solar sail spacecraft. Initial work involved the development of a 2-D deployment model capable of capturing rotation around a single axis and with the capacity to describe the extrusion process with a single described

asymmetry. While this initial step was useful for gaining confidence in the available software tools, it was evident from the beginning that numerous phenomena could not be captured by such a model. The expansion to a full 3-D deployment model allowed for the introduction of effects such as spin stabilization, and the more complicated effects of the rotor-like boom structure. The modularity of the 3-D model stems from the original derivation of the spacecraft dynamics as rigid-body rotating in inertial space. It is then possible to add flexible modes to the overall dynamic model by appending a new set of equations, coupled to the first by certain terms inherent to a spinning rotor. With careful consideration it should be possible to expand the existing model in this fashion until a desired number of flexible modes are ultimately reached, although the associated level of complexity would balloon rapidly. Current research is focused on the initial rigid-body model and a single flexible mode associated with each boom.

1. Rigid-Body Dynamics

An unusual feature of the deployment problem is the existence of time-varying mass-moments-of-inertia in the body-fixed frame. Additionally, with the possibility of asymmetric deployment, the center of mass of the spacecraft will drift. Beginning from the textbook definition[8] for the rotational motion of a body:

$$\{M\} = \frac{{}^{i}d}{dt}\{H\} \tag{1}$$

where $\{M\}$ is the externally applied moment and $\{H\}$ is the angular momentum of the spacecraft, each about the center of mass in the body-fixed frame. Substituting for the angular moment, the rotational motion of the body can be described by:

$$\{M\} = [I^b]\{\dot{\omega}^{bi}\} + [\dot{I}^b]\{\omega^{bi}\} + \{\omega^{bi}\} \times [I^b]\{\omega^{bi}\} \tag{2}$$

Equation (2) introduces $[I^b]$ as the mass-moment-of-inertia of the spacecraft at the center of mass and $\{\omega^{bi}\}$ as the angular velocity described in the body-fixed frame of the spacecraft, where "dot" terms refer to derivatives with respect to time.

The spacecraft is shown relative to the body-fixed frame in Figure 4, with the spacecraft axes defined by the plane of the undeformed booms and inline with the cruciform booms. The third body axis is fixed perpendicular to the undeformed sail-plane, with the origin of all three axes set at the spacecraft center-of-mass. An unfortunate side effect of this axis definition is that a principal axis system is no longer used, but the collocation with the center of mass is still captured. The reason for abandoning the principal axis orientation is to maintain a simple geometric orientation of every component in the body, so that properties can be readily computed. Additionally, this poses no compromise to Equation (2) as long as $[I^b]$ and its time derivative are correctly calculated in the chosen body-fixed frame.

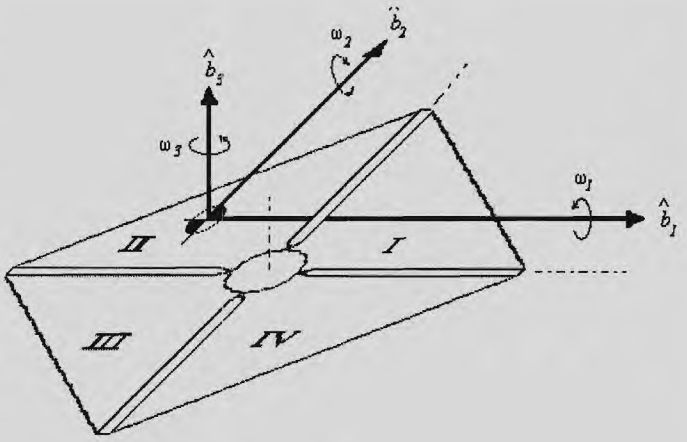

Figure 4. Definition of solar sail body-fixed frame.

The force acting on the sail is computed directly by consolidating the solar pressure on each quadrant as a total applied force acting through the center of pressure and normal to the plane of the individual sail quadrant (reference Fig. 4). This is converted to the moment contributed by each quadrant by then taking the cross product with the distance between the quadrant center of pressure and the sail center of mass, and then summing the result for the total externally applied moment, M, in Equation (2). The labeling of quadrants (reference Fig. 4) follows a standard Cartesian system for the given body axes.

2. Flexible Dynamics

The introduction of flexible dynamics, presents a considerable challenge, and the approach taken follows that used for a helicopter rotor. Equation (1) is once again utilized, this time with $\{H\}$ representing the momentum vector of the individual booms and $\{M\}$ representing the sum of the moments at the pivot point of each boom. This approach yields three equations for each boom, although due to the hinge conditions imposed on the pivot point only one is necessary for each. An unfortunate complication in the model formulation is the need to consider the relative motion of the bus and the center-of-mass, and this introduces a coupling between the flexibility of the booms, that is represented by the time-derivative of the bus angular velocity with respect to the center-of-mass. Analysis of the rigid model's behavior showed that the rate of drift in center of mass, even with a large twin-asymmetry, was extremely small and as a result the associated coupling terms in the flexible equations are multiple orders of magnitude smaller than the dominant relationship. Additionally, the decay of ω_3 due to extrusion was observed to be quite small in comparison to its magnitude. It would seem, then, that it is reasonable, in the first-order model, to neglect the two features that make this problem unlike a flapping rotor, and simply use the decoupled flapping rotor equations for each boom given by:

$$M_A + M_{CF} + M_{COR} + M_I + M_R + M_{BA} + M_{BL} = 0 \tag{3}$$

Where M_A is the applied moment on each boom due to solar pressure transferred from the adjacent sail quadrants, M_{CF} is the moment due to centrifugal force, M_{COR} is the moment due to Coriolis acceleration, M_I is the moment due to boom inertia, M_R is the moment due to the restraint at the pivot, M_{BA} is the moment due to body angular acceleration, M_{BL} is the moment due to body normal acceleration. For a given boom by substituting the general equations for each constituent moment and simplifying, Equation (3) becomes:

$$\ddot{\beta} = \frac{M_A}{I_\beta} - \frac{K_\beta \beta}{I_\beta} + \frac{m_\beta}{I_\beta}\left(\dot{W} - U\omega_2 + V\omega_3\right) - \omega_3^{\,2}\cos\beta\sin\beta + (\dot{\omega}_2 + 2\omega_1\omega_3)\cos\Psi + (\dot{\omega}_1 - 2\omega_2\omega_3)\sin\Psi \tag{4}$$

The new terms seen in Equation (4) are defined by the subscripted *I*, *m*, and *K* terms and refer to the mass-moment-of-inertia, mass, and restraint stiffness respectively of the particular flapping boom (deployed boom and tip are included in this calculation). The angle β is defined as the deflection angle due to flapping, positive downward, and Ψ is the azimuth angle of the boom with respect to the defined x-axis of the spacecraft. The *U*, *V*, and *W* terms come from the need to describe the motion of the body as a whole and are defined as the velocity vector of the spacecraft relative to the inertial origin. The need for these terms requires a modest addition to the previously defined rigid-body model, as it is now necessary to know the acceleration and velocity due to solar pressure, where before only pure rotation was required. It should be noted, that while the azimuth angle in a typical rotor problem is changing for the case of a spinning blade, the four booms comprising the square solar sail each have a fixed azimuth that is well known in the problem formulation, further simplifying Equation (4) as it is used specifically for each boom. Additionally, the eccentricity of the pivot point with respect to the rotating center-of-mass has been neglected, to remove the need for a reformulation of Equation (4) with the consideration of a 3-D eccentricity. This omission is a clear candidate for revision in future work.

While it is necessary to make numerous simplifications to describe the flexible solar sail as a flapping rotor blade, the benefit of abstracting a relatively unique spacecraft into the realm of well-known rotor mechanics solutions is clear. Additionally, with the derivations behind the equations readily available, additions to the complexity of the problem should be feasible, and while tedious and time consuming, a modest level of model fidelity can be reached.

C. State-space Representation

The computational capabilities of the Matlab software naturally led to the use of the state-space method to convert the equations of motion to a set of first-order differential equations that could be integrated in Simulink.[9] Just as it was possible to derive a modular system of dynamic equations, it is equally useful to develop a state-space representation of the system readily capable of expansion or truncation as desired.

1. Rigid-Body States

Choosing state variables for the rigid-body equations of motion follows naturally from the need to find the angular velocity of the body and the desire to know the attitude in the inertial-frame. Due to the relative motion between two frames of reference, $\{\omega^{bi}\}$ is not directly given by the first time-derivative of the attitude provided by the Euler angles. Consequently a transformation must be determined using the Euler angles themselves.

$$\left\{\omega^{bi}\right\} = \begin{bmatrix} -\sin\psi_2 & 0 & 1 \\ \cos\psi_2 \sin\psi_3 & \cos\psi_3 & 0 \\ \cos\psi_2 \cos\psi_3 & -\sin\psi_3 & 0 \end{bmatrix} \left\{\dot{\psi}\right\} = [T]\left\{\dot{\psi}\right\} \tag{7}$$

The column matrix $\{\psi\}$ is made up of Euler angles with *1, 2,* and *3* subscripts referring to yaw, pitch, and roll angles, respectively (reference Fig. 2). Equation (7) provides a useful relationship between two desired quantities and makes it clear how the desired state variables will actually be defined:

$$\begin{aligned} x_1 &= \{\psi\} \\ x_2 &= \left\{w^{bi}\right\} \end{aligned} \tag{8}$$

The first derivatives of the state vectors are given by:

$$\begin{aligned} \dot{x}_1 &= [T]^{-1} x_2 \\ \dot{x}_2 &= \left[I^b\right]^{-1} \left\{\{M\} - \left[\dot{I}^b\right]\{x_2\} - \{x_2\} \times \left[I^b\right]\{x_2\}\right\} \end{aligned} \tag{9}$$

The second portion of Equation (9) is provided by substituting Equation (8) into Equation (2) and solving for the desired variable. It is now possible to compute the first-derivatives of the state variables directly and simply integrate them numerically in Matlab. For these equations a fixed-step fourth-order Runge-Kutta integration method was utilized, with very stable results.

2. Flexible States

The inclusion of a flexible mode involves the addition of three additional states in order to reduce Equation (4) to a set of first order equations, with the additional states involving the velocity relative to the inertial frame. The states are written as:

$$\begin{aligned} x_3 &= \begin{Bmatrix} U \\ V \\ W \end{Bmatrix} \\ x_4 &= \{\beta\} \\ x_5 &= \left\{\dot{\beta}\right\} \end{aligned} \tag{10}$$

and the first-order differential equations become:

$$\begin{aligned} \dot{x}_3 &= \frac{1}{m_{tot}} \{F_{tot}\} \\ \dot{x}_4 &= x_5 \\ \dot{x}_5 &= \left\{\ddot{\beta}\right\} \end{aligned} \tag{11}$$

with the first-order equation for x_5 based on Equation (4), with individual boom values substituted appropriately, and with azimuth specified as follows:

$$\begin{aligned} \Psi_1 &= 0^0 \\ \Psi_2 &= 90^0 \\ \Psi_3 &= 180^0 \\ \Psi_4 &= 270^0 \end{aligned} \tag{12}$$

the resulting set of five first-order differential equations provided by Equations (9) and (11) lend themselves to convenient integration in Matlab, again using a fourth-order Runge-Kutta integration algorithm with satisfactory numerical stability.

III. Simulation

The simulation consisted of the implementation of Equations (9) and (11) in Matlab m-files with integration performed using Simulink. This structure lent itself well to the expansion from a rigid-body model, utilizing Equation (9) exclusively, to a first-order flexible-body model involving all of the equations described thus far (seen in Figure 5). The use of a powerful interpreted language like Matlab was appealing, but an unfortunate consequence of the use interpretive programming languages is the long execution time.

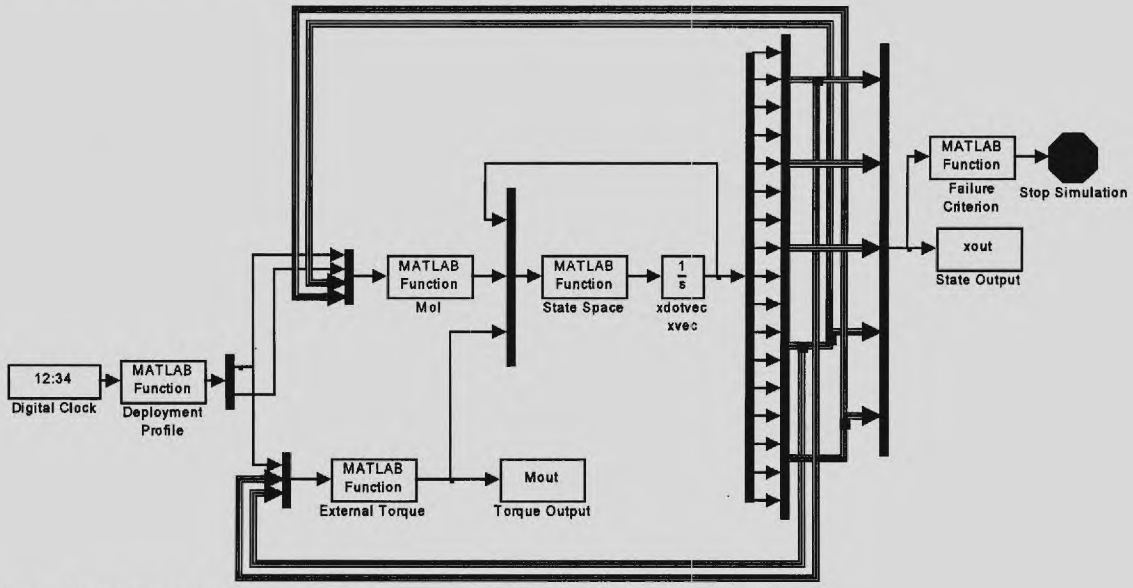

Figure 5. SIMULINK diagram for flexible solar sail deployment model.

A. Model Verification

The modular approach to the problem, depicted in Figure 5, allowed for extensive verification throughout the development process. As individual modules were developed, they were each tested to verify that they produced the expected outcome for a given set of circumstances. Specifically, all mass-moment-of-inertia functions were shown to return positive-definite matrix outputs. The function computing center-of-mass offset was verified to provide the correct offset for a given asymmetric geometry due to the complex assortment of constituent components. Additionally, sign conventions were checked for validity, ensuring that a given applied moment provided the expected changes in orientation.

After the internal components had been verified, it was possible to check the validity of the larger model. Initial validation was performed on the rigid-body model by first ensuring that a symmetric deployment did not develop a

moment due to center-of-pressure offset for the center-of-mass (would be zero for true symmetry) and that it did not alter its orientation at all as a result. Additionally, the zero asymmetry condition was given an initial spin (ω_3, reference Fig. 4) to verify that this spin would simply deteriorate due to extrusion without causing spin about any other axis. It was then prudent to verify that the outcome of a given single asymmetry would be identical no matter which boom was chosen to be different. Verifying that the roll induced around the b_1-axis was identical to the pitch induced about the b_2-axis was important not only for verifying that the Euler angles commuted in the presence of a single rotation, but also the direction of asymmetry did not affect the final result. If the opposite were true it would be tantamount to a flight dynamics problem where the heading was of consequence, a conclusion that would clearly be incorrect. A twin asymmetry was also tested to demonstrate that the presence of two moments will cause spin around all three axes. All of the above results confirmed the validity of the rigid-body model when verified against the expected outcome of the expansion of Equation (2), where it is easy to recognize what conditions cause changes in the spin about each axis.

The verification of the flexible model was slightly more involved. With so many components to Equation (4) it was necessary to test situations that would involve as few pieces as possible until confidence was gained that the appropriate outcome occurred. The first step was to verify that expected outcome of the applied moment at the reaction of the spring at the root used as an approximation for the first degree of boom flexibility. This was accomplished by testing a situation where all values for angular velocity were set to zero, and the expected result of an oscillator with no damping was seen. Next, the effect of body-normal acceleration was checked by removing the M_{BL} term from Equation (3) and observing the result. As expected the absence of this moment showed an increase in boom deflection, reflecting the fact that as the spacecraft accelerates due to the continuously applied load the moment seen at the pivot point is effectively reduced.

The effects of the moment induced by centrifugal force were observed by spinning a symmetrically deployed spacecraft and noting that the deflection of the boom was reduced throughout the deployment process, with the final oscillation occurring around a lower average value. The result is shown in Figure 6 where the anticipated result is clearly depicted. The effect of Coriolis forces were difficult to evaluate but were present while the spacecraft was under the influence of rotation around multiple axes simultaneously. Additionally, the effects of the moment due to body angular acceleration were observed to produce satisfactory results.

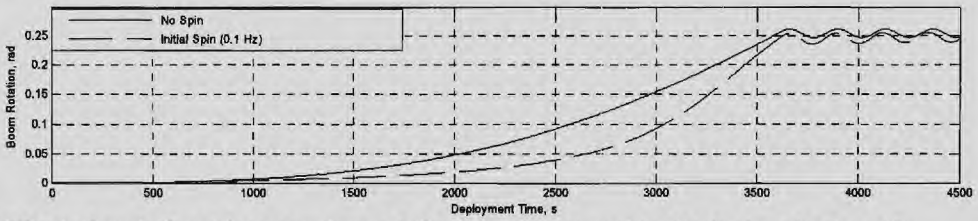

Figure 6. Effect of centrifugal forces on boom deflection of a symmetrically deployed solar sail.

B. Simulation Results

The desired outcome of the research effort is to define the conditions necessary for a successful deployment while taking into consideration a range of possible deployment problems. For the purposes of initial data gathering and analysis, nominal deployment criteria were required because an open-ended range of configurations were available to choose from. The nominal deployment time chosen for all work was 3600 seconds. The mission requirement for this style of spacecraft has a hard upper limit of two hours for a completed successful deployment due to the heating and pressurization requirements. This implies that the portion of deployment involving unpacking and extrusion must be achieved significantly sooner, allowing the verification of success and the eventual dissipation of any structural excitations induced by extrusion and external forces. To provide an ample window for such opportunities a nominal deployment time of one hour (3600-s) was chosen, as this was seen as a reasonable compromise between the upper limit and the potentially faster deployments possible if higher levels of pressurization were used to induce more rapid extrusion. Clearly, it is beneficial to deploy as quickly as possible to reduce the window of time in which the spacecraft can be affected by asymmetry. As such, one hour also presents a "worst-case" when compared to the faster rates that might be possible.

Boom 1, shown in Figure 7, was chosen to possess the nominal boom length at all times with extrusion asymmetries possible in the other booms. This choice is, of course, arbitrary as the earlier validation showed that any occurrences are ultimately free from bias as to which boom was asymmetric. Another important distinction is that, while any set of asymmetries can be chosen for use in the simulation, only two classes of asymmetry were

studied. The first is the choice of boom 2 (reference Fig. 7) as a single asymmetric boom with the length of asymmetry defined as A and taken to be longer than the other three booms. This type of asymmetry develops a single moment, about the b_1-axis (reference Fig. 4) and, if no initial spin is present, only causes rotation about one axis. The second configuration chosen for analysis is that of a twin asymmetry in which booms 2 and 3 are both longer than boom 1 by length A (reference Fig. 7). While this does present a plane of symmetry on one diagonal of the body, it was a more natural first step than introducing further parameters at this point of the research. Additionally, choosing the two booms at the same length, means that the moment developed around each axis will be maximized, enforcing the "worst-case" approach desired in this type of analysis.

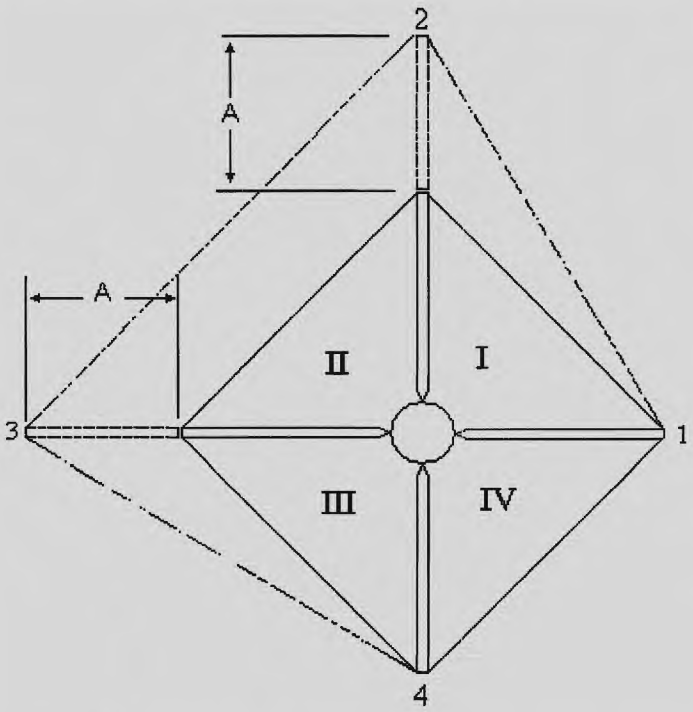

Figure 7. Definition of chosen asymmetries.

It should additionally be noted that a given asymmetry during the simulation was fixed for the entire deployment process, i.e. all four booms were given an identical rate of extrusion, with the chosen initial asymmetry present for the full length of deployment. This process assumes that as the boom pressurizes following initial unpacking it is subjected to a step asymmetry that is then maintained. While other types of asymmetry are possible (i.e. different extrusion rates), all will produce a change in the offset between the center of pressure and center of mass. Since the focus of current research is on the development of trends associated with this offset, the end result of any type of asymmetry should all lead to the same conclusion, allowing for the chosen conventions to provide general results for the given problem.

It was necessary to find a useful value for stiffness in the flexible model. A trade study (reference Fig. 8) was performed for the deployment of the flexible model with no asymmetry present with *Bending Failure* defined by the bending slope exceeding 12°, effectively placing the current model outside the limitations imposed by its defining assumptions. It was noted that acceptable levels of bending were present in the steady-state solution for the stiffness value of K = 2.9619 N-m/rad. With the stipulation that the boom is only 1-*m* long, this value lies very close to the initial computed stiffness using the approximation for flexural rigidity of the boom based on the modulus of the lining material and the area-moment-of-inertia of the boom cross section. Clearly, though, if such a value were mandated as a permanent flexural rigidity of an equivalent beam, once the boom has extruded to a full length of 70.7-*m* it would be very soft indeed. To mitigate this effect, the trade study yielded a value for K (shown in Fig. 8) that ensures the maintenance of a linear bending condition in the steady-state.

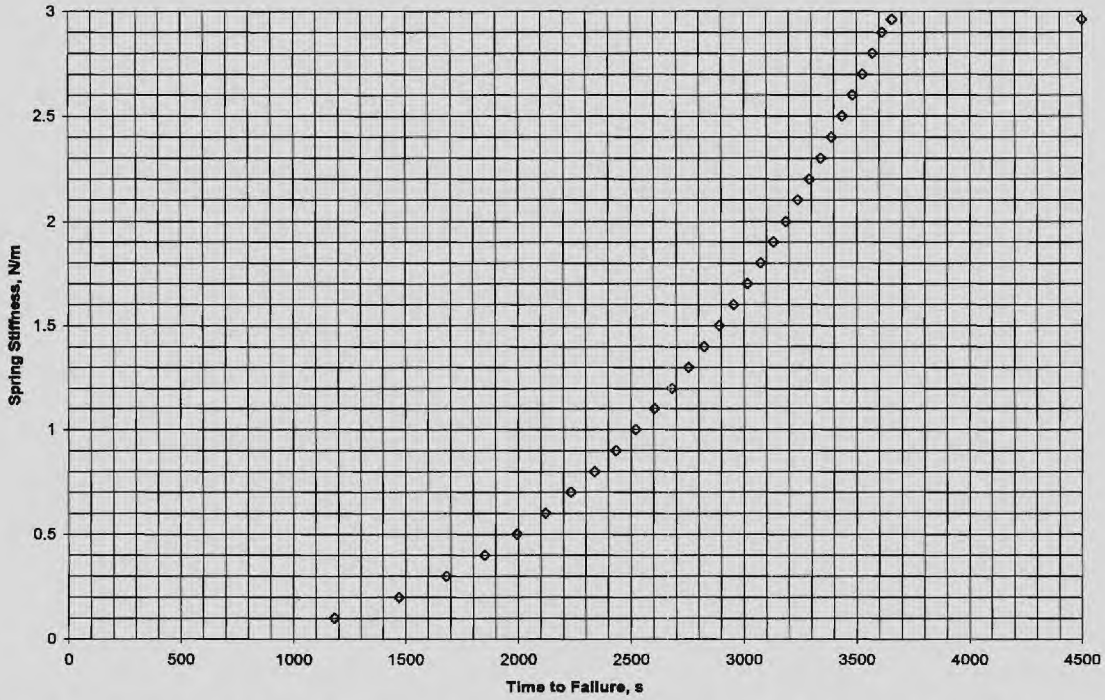

Figure 8. Required time for boom to enter non-linear bending regime with a given spring stiffness.

An important step in the process of identifying the effects of asymmetry was to discern the relationship between deployment failure and different types of asymmetry when no spin is present. Two very important correlations can be made from the results shown in Figure 9. The displayed relationship between asymmetry and deployment failure is based in the specific condition of *Orientation Failure*, in which either roll or pitch angles exceed 45°. Quite anticipated, is the result that for either the rigid or flexible model a twin asymmetry fails sooner than a single asymmetry. This expectation was expressed earlier in the discussion and reinforces the notion that twin asymmetries are more severe than a double asymmetry that does not maximize the asymmetry of both aberrant booms. The more important conclusion, and not originally obvious, is that the flexible boom will exceed the restrictions on pitch or roll sooner than the rigid body will. Important implications arise surrounding the direction of future work, as it brings to light the possibility that as the number of flexible degrees-of-freedom is increased it could considerably degrade performance. This line of reasoning could then be extended to suggest that the actual spacecraft, on which continuous bending is present, will probably perform less satisfactorily than the available models might suggest, necessitating the development a more robust deployment process to guarantee success.

Logically, it would seem prudent to investigate what might be done to increase the safety of deployment. One approach is spin-stabilization. Figure 10 shows the results of a trade study investigating the effects of initial spin about the b_3-axis to determine if such stabilization would be possible. The resulting spin rates shown are normalized to an initial configuration in which all four booms are one meter in length, in order to provide an estimate of what level of spin would be required prior to the initiation of the deployment process. The trade-study did reveal that, as expected, the required initial spin increased with the level of asymmetry, and a similar relationship between the different models and deployment conditions seen in Figure 9 is once again repeated, with the flexible spacecraft requiring more momentum to stabilize. It is worth noting that the physical geometry of the spacecraft restricts the level of asymmetry possible to far less than the 10-m extreme shown in Figure 10. As a counterpoint, though, it is once again important to recall that the offset between center of pressure and center of mass could certainly increase to a level similar to such an extreme asymmetry, by virtue of other phenomenon such as rips and tears developed during deployment. Clearly, in any situation, the moment developed about the center-of-mass will have a limit and so it should certainly be possible to spin the spacecraft to a level of stability, though the following section will delve into other surreptitious facets to deployment that may eliminate spin stabilization as an option all together.

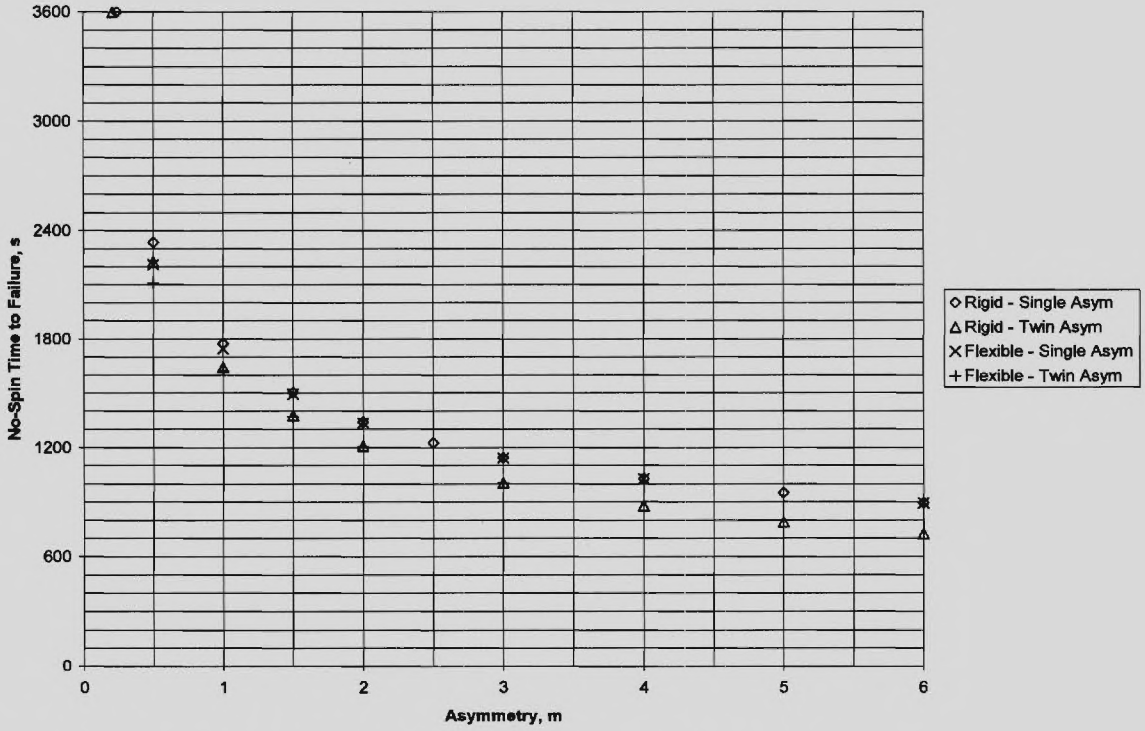

Figure 9. Deployment failure time due to asymmetry with no initial spin.

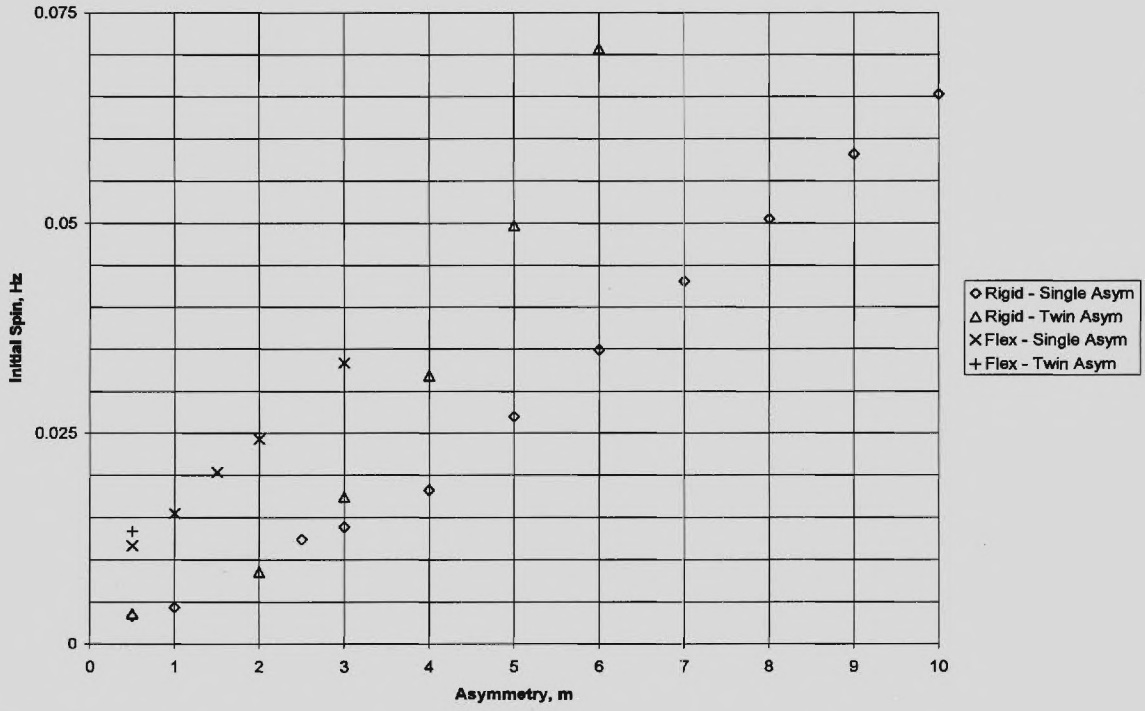

Figure 10. Initial w_3 required for a successful deployment with a fixed asymmetry.

IV. Discussion of Results

Given the trends of Figure 9 and 10 it is worth investigating other aspects of deployment in order to determine the underlying causes. Two cases were considered in this more in-depth analysis, one providing a more conclusive result for the effects of spin stabilization on the rigid model, and a second delving further into the effects of spin stabilization on the flexible body.

In the first case, a 2-m twin asymmetry was considered in order to provide a condition under which a moment was applied around two of the three body axes, with 2-m considered to be a realistic level of deployment asymmetry in practical application. With no initial spin the rigid spacecraft was consistently seen to gradually increase roll and pitch attitude until orientation failure of 45° in either Euler angle of interest was reached. This is expected due to the similarly gradual increase in the applied moment, and, in and of itself, provides no new insight.

The more interesting result stems from the behavior of the spacecraft when spin stabilization is provided. As expected from Equation (2), oscillations in both pitch and roll angle are seen, with a gradual drift toward failure at a much later time than if no spin were present. Figure 11 graphically displays the benefits of spin stabilization on the rigid spacecraft, but it is interesting to note that the roll angle varies by more than 20° peak to peak, implying that less spin may provide a satisfactory steady state outcome if transiently passing through the defined critical angle were not problematic and if the final orientation was still considered acceptable.

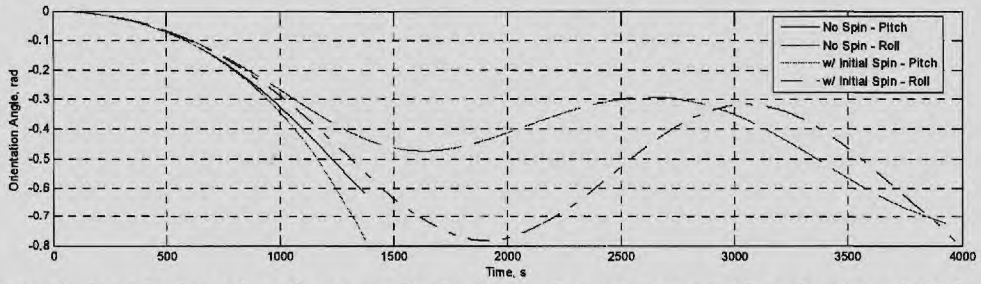

Figure 11. Evolution of orientation of spacecraft with 2-m twin asymmetry, with and without initial spin.

With assertions regarding the rigid-body model confirmed and explained, it is now possible to apply this to expand the understanding of the flexible model. Figure 12 displays the effect of spin stabilization on the attitude of the flexible spacecraft with a 2-m twin asymmetry. While nothing should lead one to believe that the body-orientation conserving effects of spin stabilization would be entirely lost on a flexible body, it is useful to make a note of it, nonetheless. It is worthy of note, as well, the considerable attenuation achieved by even a modest initial spin such as 0.01 Hz, with very little degradation in attitude seen, even two-thirds of the way through the deployment process.

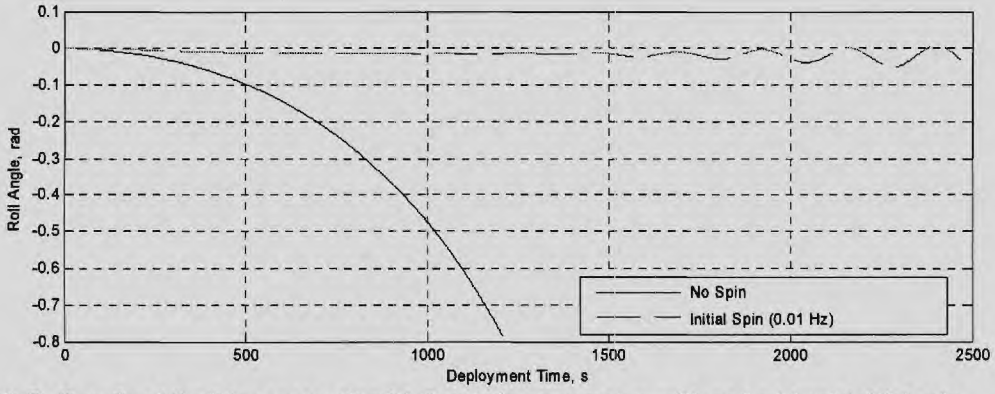

Figure 12. Roll angle of flexible spacecraft with 2-m twin asymmetry, with and without initial spin.

Figure 13 depicts the consequences of spin stabilization on the flexible asymmetric model. Unlike the symmetric case shown in Figure 6, in which the effects of spin were modestly beneficial, in the presence of asymmetry the moments due to Coriolis forces and body angular momentum come into play. A clear trend was seen that as initial angular velocity was increased, for large enough asymmetries, the magnitude of rotation exceeded the value defined for bending failure. It might be tempting to draw a correlation between the depicted increasing oscillation and the excitation of the natural frequency of the boom, but it should be recalled that the boom is evolving, continually

increasing the applied load and sustaining no oscillatory disturbances. Additionally, one of the interesting features of an evolving structure is the fact that the natural frequencies will evolve as well. This reduces the possibility of extended interaction between a disturbance and a given mode, but ultimately increases the likelihood that disturbances could coincide with a natural frequency at some point in the deployment process, if for however brief a moment. One clear aim in future work is to assess the effect of the deployment rate itself on stability of the flexible model to see if it is necessary to move quickly through certain deployment regimes to guarantee a safe deployment.

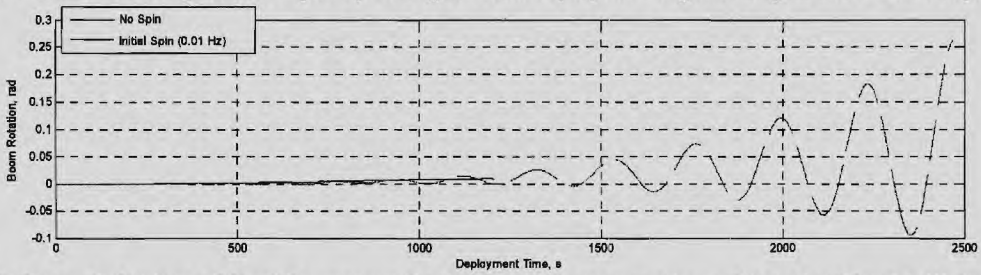

Figure 13. Boom deflection of flexible spacecraft with 2-m twin asymmetry, with and without initial spin.

The result of the comparison between Figures 12 and 13 is that, at this point, it cannot be stated conclusively that spin stabilization would be beneficial. In fact, the obvious potential exists for initial spin to become problematic to model stability. This is due to the consistent presence of potentially undesirable moments that arise from the spin about multiple axes if an asymmetry occurs. This unique feature of an evolving structure is clearly a topic for further analysis with higher order models to discover how pervasive the effects really are. It is entirely possible, however, that with this type of problem spin stabilization is not a viable option due to the fact that it consistently excites the structure in the presence of exactly the conditions it was trying to alleviate.

V. Conclusion

A simple model for the dynamic response of an inflatable solar sailcraft during deployment has been developed and tested for several distinct scenarios. The basic kinematics for the model were formulated in a deliberate manner that in future studies will allow systematic increases in model fidelity (and complexity) while at the same time leading to a straightforward implementation as a state space model in Matlab/Simulink. Despite the low order of the current model, clear trends were evident. It was shown that including flexibility in the form of rotational springs at the boom-bus interface was detrimental to the overall robustness of deployment. This suggests the need for higher order models to discover how problematic such effects could actually be. It was shown that spin stabilization, while beneficial to the rigid-body dynamics in every case, seemed to be detrimental to the flexible dynamics when angular velocity was increased above a certain initial magnitude. Again, this presents a clear path for future development and the need to investigate further what effects may contribute to the excitation of the flexible modes. Other areas to consider include orbital or gravity gradient effects to the rigid-body dynamics. Each step of the way it will be important to continually revisit these initial trends to reassess later developments as well as actively relaxing the assumptions in place to always ensure an increasing level of model fidelity.

Acknowledgments

This research was supported by the NASA Marshall Space Flight Center under a NASA GSRP award NNM05ZA02H.

References

[1]McInnes, C. R., *Solar Sailing: Technology, Dynamics and Mission Applications,* Springer-Verlag, New York, 2004, Chaps. 1-4.

[2]Clem, A.L., Smith, S.W., Main, J.A, "A Pressurized Deployment Model for Inflatable Space Structures," *41st AIAA/ASME/ASCE/AHS Structures, Structural Dynamics, and Materials Conference,* Atlanta, GA, AIAA-2000-1808.

[3]Clem, A.L., Smith, S.W., Main, J.A., "Deployment Dynamics of an Inflatable Solar Array," AIAA-99-1520.

[4]Smalley, K.B., Tinker, M.L., "Nonlinear Pressurization and Modal Analysis Procedure for Dynamic Modeling of Inflatable Structures," *Journal of Spacecraft and Rockets*, Vol. 39, No. 5, September-October 2002.

[5]Fang, H., Lou, M., Hah, J., "Deployment Study of a Self-Rigidizable Inflatable Boom," *44th AIAA/ASME/ASCE/AHS Structures, Structural Dynamics, and Materials Conference,* Norfolk, VA, AIAA 2003-1975.

[6]Sleight, D.W., et al., "Finite Element Analysis and Test Correlation of a 10-Meter Inflation-Deployed Solar Sail," *46th AIAA/ASME/ASCE/AHS/ASC Structures, Structural Dynamics, and Materials Conference*, Austin, TX, AIAA 2005-2121.

[7]Laue, G., Case, D., Moore, J., "Fabrication and Deployment Testing of 20-Meter Sola Sail Quadrants for a Scalable Square Solar Sail Ground Test System," *46th AIAA/ASME/ASCE/AHS/ASC Structures, Structural Dynamics, and Materials Conference*, Austin, TX, AIAA 2005-2125.

[8]Wiesel, W.E., *Spaceflight Dynamics*, 2nd ed., Irwin/McGraw-Hill, New York, 1997, Chap. 4.

[9]Matlab/Simulink, www.mathworks.com.